Environmental Pollution 366 (2025) 125441

Contents lists available at ScienceDirect

Environmental Pollution

journal homepage: www.elsevier.com/locate/envpol

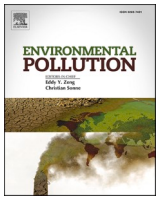

Forest fire emission estimates over South Asia using Suomi-NPP VIIRS-based thermal anomalies and emission inventory

Kumari Aditi [a,b], Akanksha Pandey [a], Tirthankar Banerjee [a,b,*]

[a] Institute of Environment and Sustainable Development, Banaras Hindu University, Varanasi, India
[b] DST-Mahamana Centre of Excellence in Climate Change Research, Banaras Hindu University, Varanasi, India

ARTICLE INFO

Keywords:
Fire
Biomass burning
Carbon emission
Inventory
VIIRS

ABSTRACT

Emission estimates of carbon-containing greenhouse gases (CO_2, CH_4) and aerosols ($PM_{2.5}$) were made from forest fire across South Asia using Visible Infrared Imaging Radiometer Suite (VIIRS) based thermal anomalies and fire products. VIIRS 375 m I-band active fire product was selectively retrieved for the years 2012–2021 over forest cover across South Asia. Annual incidence of fire events across South Asia was 0.17 (±0.05) million (M) with robust spatio-temporal variation. Fire occurrences were mainly concentrated over the forest across Hindu Kush Himalayan region (HKH; 56%), Deccan Plateau (DP) and Central Highlands (CH; 34%). Monthly mean fire incidences emphasize February to May as a typical forest fire season, accounting 90% of annual fire counts. The highest fire pixel density (>1.5 km $^{-2}$ yr^{-1}) was noted over the tropical dry/moist deciduous and tropical semi-evergreen forests. Strong diurnal nature of fire radiative power (FRP) was evident with >85% of FRP linked to daytime retrieval. VIIRS based Fire Emission Inventory (VFEI, Version 0) was followed to constitute regional emissions of $PM_{2.5}$ and green house gases from forest fire. Forest fire accounted a yearly emission of 91.58 (±14.76) and 0.25 (±0.04) Tg yr^{-1} CO_2 and CH_4 respectively, with 25.14 (±3.94) Tg of cumulative carbon release per year, i.e., roughly 1.3% of global fire-related carbon emission. Fire associated $PM_{2.5}$ emission rate was 0.60 (±0.10) Tg yr^{-1}, 95% of which emitted during peak fire season as was the case for carbon-containing gases. Forest fire across HKH (75%) and DP + CH (20%) predominately contribute to the regional carbon emission, while also accounting 68% (HKH) and 27% (DP + CH) of fire associated $PM_{2.5}$ emission budget. With >70% of forest fires within South Asia being typically anthropogenic, forest fire appears to be a major sector of greenhouse gas and aerosols emissions, and necessitate planning and strict legalities to reduce emission load.

1. Introduction

Forest areas across the world have been experiencing rising levels of fire activity and severity that are unprecedented in the historical record. Megafires have been a recurring feature in forests and woodlands negating years of greenhouse gas emission cuts (Jerrett et al., 2022; van der Velde et al., 2021). While fire has many ecological benefits, it can also endanger human and animal life, and damage infrastructure under certain scenarios (Xu et al., 2020; McLauchlan et al., 2020; Duff and Penman, 2021). Among 40.6 million (M) sq. km of global forest coverage, about 0.98 M sq. km was affected by fire in 2015, accounting 2.41% of entire forest cover (FAO, 2020a,b). In another estimate, approximately 3.4% of Earth's land surface is estimated to burn every year (Giglio et al., 2018). Such estimates, however have large bias constrained by unavailability of high-resolution burned area data product (Roy et al., 2019; Roteta et al., 2019).

Typically, forest fire occurrence has marked spatial and temporal heterogeneity with tropical forest primarily experiences frequent fire, especially in central Africa, and South and North America. Majority of these fires are intentional to clean up the forest for agriculture and other commercial purposes, particularly in Africa, Southeast Asia and in South America (Field et al., 2009; Andela and van der Werf, 2014). In contrast, wildfires in Russia and Canada are mainly natural, often fires on northern boreal forest initiate by lightning (Chen et al., 2021) while forest/bush fire in north America and Australia has a notable link with hydroclimatic and geomorphic characteristics of the forest itself (Deb et al., 2020; Moritz et al., 2005). Forest fire in South Asia is primarily sporadic, mainly evident in India, Nepal and in Bhutan, with approximately 13–15 thousand sq. km yearly forest burnt area, accounting 1.7% of total forest cover (FAO, 2020a,b; FSI, 2023). India accounts a major

* Corresponding author. Institute of Environment and Sustainable Development, Banaras Hindu University, Varanasi, India.
E-mail addresses: tb.iesd@bhu.ac.in, tirthankaronline@gmail.com (T. Banerjee).

https://doi.org/10.1016/j.envpol.2024.125441
Received 31 May 2024; Received in revised form 28 November 2024; Accepted 1 December 2024
Available online 4 December 2024

share of the South Asia forest fire with ~11 thousand sq. km burnt area in years 2019-20, close to 1.6% of total forest cover (FSI, 2020; 2023). Among different physiographic zones, Deccan (5630 sq. km) and Central Highlands (2160 sq. km) forest account 70% of total burnt area while northeast states of India, despite having higher satellite-based fire counts, accounts 13% (FAO, 2020a,b; FSI, 2020; 2023). Such heterogeneity in fire incidence is mainly linked to plant dry matter and climate, as dry deciduous and tropical evergreen forests including Eucalyptus and Pine plantations are more susceptible to forest fire compared to evergreen and montane temperate forest. In a recent estimate, 72 thousand sq. km of India's forest, i.e. 10% of total forest coverage is marked as extremely prone to fire while 252 thousand sq. km (36%) of forest as susceptible (FSI, 2019). In terms of fire incidence, 9.9% of forest land is frequently subject to fire occurrence with varying intensities while 54% of forest land occasionally exposed to forest fire (FSI, 2019; 2020). Other South Asian countries like Bhutan (average burnt area: 250 sq. km) and Nepal (4000 sq. km) accounts approx. 1.25% and 11% of national forest cover under frequent fire incidences (Bajracharya, 2002; RGoB, 2004).

Tracking forest fire and quantifying burnt area with expected emissions has never been so feasible until the introduction of geospatial technology and sensing techniques to detect thermal anomalies at micro-scale (van der Werf et al., 2017; Gale et al., 2021; Wooster et al., 2021). Initiated during 1960s as airborne thermal imagery, remote sensing of fire practically kicked off in 1980s by Advanced Very High Resolution Radiometer (AVHRR) with 3.7 μm channel. Detection of active fire and emission estimates at 1 km resolution was further advanced by the use of two 3.96 μm MIR channels in Moderate Resolution Imaging Spectroradiometer (MODIS) sensor onboard Terra/Aqua satellites. Introduction of next-generation low earth orbit sensors like Visible Infrared Imaging Radiometer Suite (VIIRS) and Sentinel-3 Sea and Land Surface Temperature Radiometer (SLSTR), with sensors in geostationary satellites like Geostationary Operational Environmental Satellite, Himawari and Meteostat further refine active fire products. Detailed discussion on the evolution of fire sensing technique and comparison of data products are in Wooster et al. (2021) and Gale et al. (2021), and references there in. Clearly, based on detection technique, fire products vary with sensor and comparison among them need additional caution. For example, VIIRS-based average fire counts over India and Nepal usually 7.5 and 10.5 times of MODIS retrievals, respectively (Li et al., 2018; Vadrevu et al., 2019). However, it is being argued that VIIRS 375 m product provide improved detection of fire due to its sensitivity towards low intensity fire, greater spatial resolution and high thermal saturation point (Vadrevu et al., 2018; 2019; Li et al., 2018).

Forest fire is an important contributor of aerosols and greenhouse gases, and induce significant interannual variability in the atmospheric abundance of these climate forcing agents on a global scale (van der Werf et al., 2010, 2017; Bowman et al., 2020; Clarke et al., 2022). Global CO_2 emissions from wildfires are roughly equivalent to one-fifth of total fossil-fuel emissions (van der Werf et al., 2017), thereby potentially establishing forest fire as a mainstream emission sector like any other conventional sources. van der Werf et al. (2017) concluded 2.2×10^9 ton of yearly global carbon emission from forest fire with major contribution from small scale fires across America, Europe and temperate Asia. Jerrett et al. (2022) argued that CO_2 equivalent emissions from 2020 California forest fire was possibly two times to the entire greenhouse gas reductions in the state since 2003. van der Werf et al. (2010) reported that the contribution of forest fire (15%) to global carbon emission was relatively less compared to fires in grass land and savannas (44%). Shi et al. (2015) reaffirmed the contribution of forest fire to the emission of several greenhouse gases and aerosols over tropical regions using MODIS based burned area product. Since these forest fires are associated with huge emissions of aerosols and greenhouse gases, this could effectively accelerate change in regional climate thereby, reinforcing feedback loop. Likewise, Abatzoglou and Kolden (2013) emphasized climate change induced fuel dryness in the forests of western North America enhances its vulnerability to fire. On the contrary, Touma et al. (2021) highlighted the possibility of aerosol-driven cooling to counterbalance greenhouse gas-induced extreme fire conditions throughout the 20th century. Relative decline in aerosol loading in 21st century over Eastern North America and Europe however, offset such regional cooling resulting to further accelerate dryness, thereby enhancing fire-weather risk. Clearly, loss of forest-locked carbon due to recurrent fires leads to jeopardy the streams of ecosystem services and goods to the society, effectively turning forest as a major source of aerosols and greenhouse gases. It is noteworthy that fraction of such emitted carbon is expected to compensate due to subsequent regeneration of forest itself except in permanently deforested zone and in peatlands.

Biomass burning inventories typically use geospatial database of satellite/surface-based thermal anomalies, and constitute the emissions of trace gases and aerosols following either a *bottom-up* or a *top-down* approach. Several *bottom-up* global/regional biomass burning emission inventories have been developed based on surface data including active fire counts, fuel type and fire burned area to infer intensity of emission sources. On the contrary, *top-down* approach utilizes satellite-based fire radiative power (FRP) and species-specific emission factor to compute emissions. It is noteworthy that for a given species, the uncertainties among the inventories can be large and may differ by a factor of 3–10 (Wang et al., 2018; Pan et al., 2020; Hua et al., 2023). Like, Bian et al. (2007) compared six biomass burning inventories for global CO resulting a 30% of deviation which could reach to 2–5 times magnitude on a regional scale. Plausible causes for such disparity could be many including simulation of missing precursors, resolution, model configuration especially on an undulated topography, and dynamics of aerosols and its precursors.

Here, likely emissions of aerosols (as $PM_{2.5}$) and greenhouse gases (as CO_2, CH_4) from forest fires across South Asia was explored using VIIRS-based active fire anomaly at I-band coupled with a high-resolution biomass burning inventory based on fire radiative power density and species-specific emission factors. To develop a mechanistic understanding of the possible contribution of forest fires on regional emissions, we employed widely used criteria to detect forest fire, track its intensity and measure fire pixel density at highest possible resolution, extending our observation to a decade to constitute long-term trend and to assess geospatial variations. Emissions of greenhouse gases and aerosols from forest fire across South Asia is not documented yet except quantifying regional fires over specific forest area (Badarinath et al., 2011; Vadrevu et al., 2012). Use of remotely sensed daily satellite product across South Asia with quality assured retrievals of thermal anomaly and fire with varying intensities is therefore, a key advancement and can serve in improved parameterization of climate and air quality models over the region.

2. Study domain, datasets and methods

2.1. Description of the study domain

South Asia is one of the most unique and complex geographical regions having many conventional sources of aerosols and co-emitting trace gases. Along with many conventional sources, fire on agriculture residues and forest contribute significantly to regional emissions of aerosols and long-lived greenhouse gases. South Asia sustains approximately 25% of world's population with mere 2% of world's forest coverage, amount to only 0.05 ha of per capita forest land (FAO, 2020). Total forest area within South Asia in year 2021 was approximately 0.9 million sq. km, accounting 19.9% of the entire geographical area (World Bank, 2024). Among the South Asian countries, India poses the maximum land under forest coverage (0.72 M sq. km., in 2021) followed by Nepal (0.59) and Pakistan (0.36) while Bhutan (71.5%) and Nepal (41.6%) ranks top in terms of percentage of land area under forest cover (World Bank, 2024; FSI, 2023; Table S1).

South Asian Forest is moderately dense to open forest type (80%)

with proportion of very dense forest is relatively less (20%). A broad range of eco-climatic zones can also be noted within South Asia, with forest types ranging from tropical wet/semi-evergreen rainforests, tropical and sub-tropical deciduous forests, temperate and sub-temperate forest and desert jungles. As in Fig. 1, for comparative analysis among different forest systems, forest over South Asia was classified into Hindu Kush Himalayan (HKH) ranges of northern Pakistan, north-western India, Nepal and Bhutan to Indian state of Arunachal Pradesh, over the parts of north-east India and south-east Bangladesh; central and eastern parts of India over Deccan Plateau and Central Highlands (DP + CH); in western Ghats (WG) and in Sri Lanka (SL). Diversity in climate, geology, soil quality and topography across South Asia leads to rise in diverse forest types. Likewise, tropical rain forest is prominent across Western Ghats, in northeast India, Sri Lanka and in the Andaman Islands. Tropical dry deciduous and dry evergreen forests present in the sub-Himalayan regions, in central and southern peninsula. Subtropical broadleaf and dry evergreen forests predominate in Himalayan range, and in northeastern and southeastern India (Ramakrishnan et al., 2012).

2.2. MODIS land cover

The latest Terra/Aqua MODIS L3 V6.1 Global Land Cover type product (MCD12Q1) at 0.5 km resolution was retrieved from LAADS DAAC site for years 2012 and 2017, to assess forest cover over entire South Asia. The MODIS land cover type is constituted based on supervised classification of MODIS reflectance coupled with prior ancillary information. MODIS land cover classification algorithm adopts forest classification scheme of International Geosphere-Biosphere Programme (IGBP) and other land type classification schemes. Here, land cover classes with value 1 (Evergreen Forest) to 9 (Savannas) was included as forest land, excluding only the land cover demarcated as shrublands. The years 2012 and 2017 were chosen to delineate the forest cover boundary assuming gradual changes in forest cover over time across South Asia (as in Table S2).

2.3. VIIRS active fire anomaly product

Launched under National Aeronautics and Space Administration (NASA) and the National Oceanic and Atmospheric Administration (NOAA) partnership, the next generation polar-orbiting operational environmental satellite system is currently on orbit under Joint Polar Satellite System (Goldberg et al., 2013; Schroeder et al., 2014). These polar satellites, in continuing the MODIS and MISR legacy, provide critical information on earth system science and improve numerical forecasting of weather and air quality. The VIIRS, a next generation scanning multispectral radiometer, was initially launched in October 2011 aboard the Suomi-National Polar-orbiting Partnership (S-NPP) satellite and subsequently in NOAA-20 and NOAA-21 satellites. The VIIRS is instrumental in providing Environmental Data Records (EDR), columnar aerosol loading (DB/DT AOD) and active fire products at different resolutions. For active fire detection, VIIRS typically extends the MODIS Fire and Thermal Anomalies algorithm (MOD14 and MYD14), initially at 750 m (M-bands) using dual gain midwave infrared channel (4 μm) and a single gain thermal infrared (11 μm) channel data (Csiszar et al., 2014). The I-band based 375 m VIIRS active fire detection algorithm (Schroeder et al., 2014; Oliva and Schroeder, 2015) however, uses brightness temperature on middle (3.55–3.93 μm) and thermal infrared regions (10.5–12.4 μm), and is reported to perform better in capturing low intensity fires and to track fire growth (Schroeder et al., 2014).

The VIIRS sensor on board Suomi National Polar-orbiting Partnership (Suomi NPP) is a cross-track single-angle scanning radiometer that flies in a sun-synchronous orbit with equator crossing at ≈1:30 p.m. and ≈1:30 a.m. local time. Due to its wide swath (~3000 km) and on-board pixel trimming algorithm, it provides global images of active fire on daily basis with better coverages on lower latitude. Owing to its better sensitivity towards low intensity fires and greater accuracy in detecting active fire, SNPP VIIRS 375 m (I-band) Collection-2 Level-1B VNP14IMG product was used to detect fires over the demarcated forest areas of South Asia in between January 2012 and December 2021, except monsoon months (July–Sept.). Among the fire mask SDS classes, only the nominal and high confidence fire pixels were taken into account avoiding potential contamination of low-confidence pixels with sun glint and low relative temperature anomaly at mid-infrared channel.

2.4. Fire radiative power

Fire radiative power (FRP) is used to define fire intensity and to

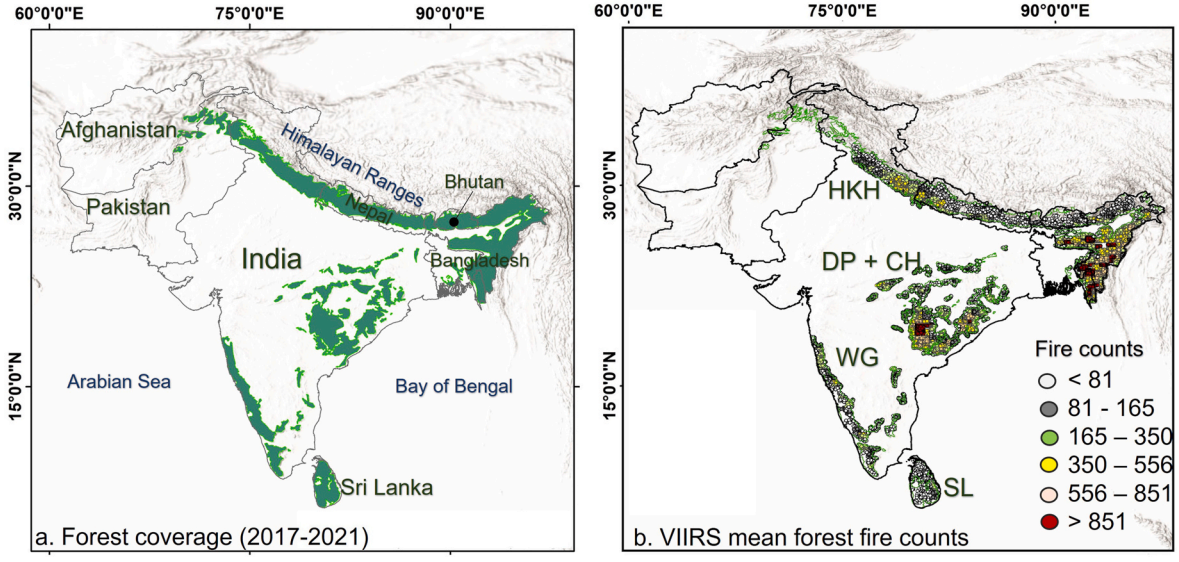

Fig. 1. Spatial domain selected for retrieval of VIIRS thermal anomaly and fire data, (a) forest cover across South Asia based on MODIS land cover classification product for year 2017, and (b) spatial variations of decadal mean fire incidences at 10 × 10 km grid across forest biomes over South Asia.
NOTE: In Fig. 1a, forest cover considering MODIS land cover year 2017 was depicted with green border while forest cover considering MODIS land cover 2012 is in supplementary file (Fig. S1). To denote spatial heterogeneity of forest fire incidence, fire counts is plotted in Fig. 1b. The background image indicates the hill shade. HKH: Hindu Kush Himalaya; DP + CH: Deccan Plateau and Central Highland; WG: Western Ghats and SL: Sri Lanka.

capture the amount of radiative loss of energy from the biomass burning. FRP is frequently used as a proxy for measuring biomass consumption and smoke emissions through forest fire (Kaufman et al., 1998; Wooster et al., 2003; Nguyen and Wooster, 2020), to assess fire behavior and growth (Smith and Wooster, 2005), and in certain cases used to quantify emission from biomass burning (Ichoku and Kaufman, 2005) both for aerosols and green-house gases (Kumar et al., 2011; Vermote et al., 2009). FRP is measured in terms of radiative fire power (MW/pixel) and can be integrated over time and space to compute fire radiative energy (mega joules, MJ). Both MODIS and VIIRS provide FRP using similar approach and has been briefed in Wooster et al. (2003) and Li et al. (2018). Briefly, both sensors utilize 4-μm band fire pixel radiance, background radiance of non-fire pixel, atmospheric transmittance and a sensor specific coefficient. For this analysis, FRP (in MW) was retrieved from the SNPP VIIRS C2 Level-2 (L2) 375 m active fire product (VNP14IMG) over the selected region of South Asia. The VNP14IMG relies on MODIS Thermal Anomalies and Fire algorithm using ~6-min orbital segments from several VIIRS scans. Clearly, VNP14IMG FRP product poses higher resolution and is more equipped to handle abnormal radiance in mid-infrared band compared to MODIS due to fewer pixel saturation. Here, FRP was used to detect fire over forest land, track fire intensity, to constitute trend in fire over forest land and was finally linked with emission of greenhouse gases and aerosols from wildfire. VIIRS FRP was further used to measure fire radiative energy integrating pixel-based FRP over spatio-temporal scale.

2.5. VIIRS-based fire emission inventory

With concurrent improvements in understanding of atmospheric dynamics of aerosols, its precursors and other greenhouse gases, and by the availability of higher computation facilities, biomass burning inventories are now grown-up to be more accurate with the ability to provide high-resolution output on a global-scale. Among the *top-down* approaches, VIIRS based Fire Emission Inventory (VFEI, Version 0) by Ferrada et al. (2022) is novel based on the fact that it delivers daily emission fluxes at a resolution of 0.005° (0.5 km) for 46 species including greenhouse gases and aerosols. The VFEI utilizes thermal anomaly product from VIIRS on board Suomi-NPP with possible inclusion of fire product from NOAA-20 in future update. The core configuration of VFEI is based on using FRP density computed from middle and thermal infrared imagery from VIIRS I-band (Schroeder et al., 2014; Csiszar et al., 2014). This enables VFEI to detect small intensity fire more accurately compared to VIIRS M-band (0.75 km) and MODIS fire detection data product (1 km). Besides, greater swath of VIIRS sensor (~3040 km), less dependency on view zenith angle (Wang et al., 2018; Li et al., 2018) and higher saturation temperature against MODIS (Polivka et al., 2016) also help VIIRS I-band to deliver better thermal anomaly product. The biomass burning emission factor included in VFEI is based on emissions compiled by Andreae (2019) on six different biomes, following several experimental outcomes on open biomass burning emissions including in-field campaigns. Sensor-specific conversion factor applied on VFEI was the result of Heil et al. (2010) based on linear regression on MODIS FRP and biomass-combustion from GFED (V3.1). Both conversion factor and emission estimates are assumed to be climatologically representative of each biome, constrained using IGBP and Köppen climate classifications, and also adopted in VIIRS land cover classification product. Here, VFEI emission estimates on aerosols ($PM_{2.5}$) and greenhouse gases (CH_4 and CO_2), available at 0.5 km resolution, were extracted over pre-selected forest cover across South Asia to constitute geospatial trend, to compare zonal disparity in emissions, and to relate possible implications on regional air quality and climate.

2.6. Geospatial analysis of forest fire emission

The study focused explicitly on quantifying forest fire incidences in all forest biomes across South Asia and associated emissions of greenhouse gases and aerosols. Initially, Terra/Aqua MODIS L3 Global Land Cover type product was processed for two years, 2012 and 2017, to account for any change in regional forest cover with time. Land cover classes marked with 1–9 were selectively considered under forest cover and a regional forest area map was created. Four specific forest zones were further segregated from the entire forest cover, namely HKH, DP + CH, WG and SL to identify spatial heterogeneity in fire incidences and emissions. The SNPP VIIRS 375 m I-band active thermal anomaly and fire product was used to retrieve fire pixel and associated FRP, constrain by day and night satellite overpass, across all the selected forest systems. Both fire counts and FRP was initially processed for day and night, before aggregating it to constitute day-to-day and seasonal variations. The ratio between day-night aggregate fire pixel with unit area of the respective grid cell was computed to assess fire pixel density following the methodology as in Giglio et al. (2006). Both fire counts and FRP were compared spatially among the selected biomes and for individual months to assess heterogeneity in forest fire. The non-parametric Mann-Kendall test with Theil-Sen's slope was applied on annual mean fire counts to determine the geographic trend of fire incidences. To constitute emission of greenhouse gases and aerosol emission from forest fire, VIIRS based Fire Emission Inventory (VFEI, Version 0) by Ferrada et al. (2022) was considered because of its dependence on VIIRS I-band thermal anomaly product which are reported to be sensitive for large fire, having finer resolution and broader swath. Emission flux estimates of the forest cover across South Asia were computed based on product of fire pixel density, emission factors and conversion factor on a daily basis, averaging day-night overpass of VIIRS and applying several static corrections to the active fire product. Emission flux (as in kg m^{-2} s^{-1}) of designated greenhouse gases and aerosols ($PM_{2.5}$) over selected fire hotspots was initially summed up daily basis to account cumulative emission, before computing spatial and temporal gradient. Emissions of greenhouse gases and aerosols were initially estimated for the all the forest cover across South Asia, before subject to regional analysis. Geospatial analysis of the emissions from the designated forest biome was also made to assess the signature of regional emission present within diverse forest type across South Asia.

3. Results and discussion

3.1. Spatial distribution of forest fire

Annual variations in fire counts in the forest across South Asia is shown in Fig. 2a. Annual aggregate fire counts over South Asia and individual forest biomes are indicative of regional heterogeneity in fire incidences between the years 2012 and 2021. Geospatial average of every single fire count detected by VIIRS across South Asia yield marked spatial heterogeneity that too varying considerably with time (Table S3). Likewise, yearly average (±SD) fire counts over South Asia was 179529 (±46107) having median counts of 0.17 million (M) within a range of 0.11–0.26 M fire incidences. Yearly time-series of fire incidences revealed robust interannual variations at the regional scale. Almost 56% of fire counts over South Asia was associated with the Hindu Kush Himalayan Forest (HKH), transverse from northern mountain of Afghanistan to Himalayan ranges till the tropical forests of northeast India. On an average 99625 (±28465) fire events were retrieved yearly across the HKH forest with range varying from 0.06 to 0.15 M, having median fire counts of 0.09 M.

In terms of proportion to total fire occurrence, HKH forest share the major fraction of fire incidence (55–67%) throughout the monitoring period. Such high incidences of fire across HKH are possibly linked to rising temperature, human perturbations, decline in precipitation and snowfall, leading to change in forest ecology (Mina et al., 2023). However, in 2017–2018 fire season cumulative fire counts dipped in HKH compared to Deccan Plateau (DP) and Central Highlands (CH). Interestingly, deciduous forest of HKH often leads to small and limited fire incidences due to greater humidity in root zone compared to coniferous

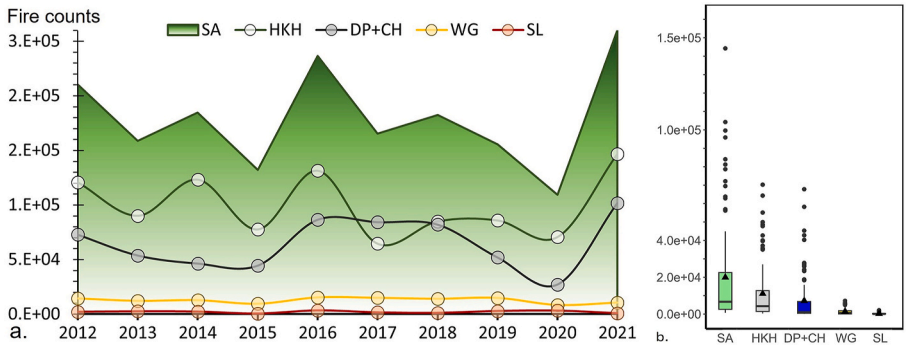

Fig. 2. Time-series of annual forest fire counts (a), and distribution of monthly forest fire counts within each forest system across South Asia (b).
NOTE. In Fig. 2b, triangle and horizontal line indicate the mean and median, respectively.

forest where high resin and dry biomass often leads to formation of intense and major fires (Negi and Dhyani, 2012). VIIRS based thermal anomalies does indicate the prevalence of high fire counts over the DP and CH region (65106 ± 23735) with median fire events of 0.06 M per year, accounting 36% of average fire incidences of entire South Asia. The tropical dry deciduous forests over DP and CH were reported to be extremely vulnerable to fire incidence (FSI, 2020). According to the FSI (2020) technical report, based on randomly selected forest fire zones, Central Highlands, Deccan Plateau and Eastern Ghats together account the highest proportion of forest affected with fire (79.7%), followed by Himalayan Forest, including northeast India (14%). Majority of these fire occurrences are strongly modulated by the biomass density, moisture content of the dry vegetation biomass, high temperature and precipitation (Prasad et al., 2008). Rest of the forests i.e. in Western Ghats (WG) and in Sri Lanka (SL) were comparatively less prone to fire with yearly mean fire incidence of 12743 (±2423) and 2055 (±965), respectively. A MK trend analysis on annual fire count over individual forest cover indicates non-significant trend in fire incidences across all the zones over South Asia.

3.2. Spatial variations of fire season

Forest fire counts constrained by months across South Asian biomes are plotted in Fig. 3 with an indication of the period having peak fire incidences between 2012 and 2021. Monthly mean fire counts across the forest system indicate that fire incidences typically rise during the month of February before reaching to its maximum in March irrespective of geographical region.

An approximate 170% increase in mean fire counts in February compared to its precedent month clearly mark the initiation of the fire season over South Asia. Interestingly, increase in fire counts was spatially inconsistent with prominence over the central and southern region of the continent compared to the northern part. Monthly fire incidence reaches to 15752 (±8334) during February, mainly driven by the increased fire counts over HKH (7284 ± 2907) and in DP and CH (4987 ± 4506). A five time increase in fire occurrence was further accounted during March (SA: 77271) compared to February (SA: 15752) was consistent with the previous reports of fire occurrence in South Asia (FSI, 2020; 2023; Prasad et al., 2008; Mina et al., 2023). Increase in fire counts was specifically evident across the Himalayan Forest (470% increase), and in Deccan Plateau and Central Highlands (510%) while an identical trend, although much lower in intensity, can also be noted over the mountainous forest in Western Ghats. This clearly marked the month of March having the most fire incidences and associated risks over the South Asian Forests, possibly linked with changes in hydroclimatic and geomorphic characteristics of the forest itself (Deb et al., 2020; Moritz et al., 2005). Quantifying the association between fire incidence and fuel moisture, vapour pressure deficit and other meteorological parameters can therefore, serves as a possible indicator of the exceeding incidence of fire during pre-monsoon season. On the contrary, forest fire occurrence at Sri Lankan (SL) island were high both in March (459 ± 370) and October (598 ± 777), much associated to human induced fire incidences compared to more of natural origin of forest fire at mainland South Asia. Overall, compared to typical forest fire season i.e. February to May, incidences of forest fire across South Asia were less during June to January, accounting only 10% of yearly fire events.

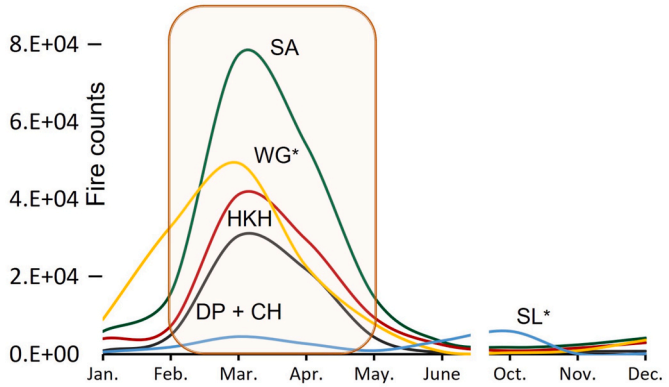

Fig. 3. Identifying peak forest fire incidence season across biomes over South Asia.
NOTE. The lines were smoothed for better visualization. Monthly mean fire counts in WG and SL were represented as *10.

3.3. Spatial variations of fire density and fire radiative power

Fire pixel density was estimated at 0.1° grid to identify and sort forest cover in terms of frequency of fire incidence as retrieved by VIIRS I-band. Fire pixel density was assessed following the protocol as discussed in Giglio et al. (2006) and adopted by Li et al. (2018). Briefly, the ratio between day-night aggregate fire pixel against the area of the respective grid cell was computed and plotted in Fig. 4 following two separate time-constrained forest coverage over South Asia based on MODIS land cover product. The highest fire pixel density (>1.57 count·km $^{-2}$· yr^{-1}) was noted over the tropical dry/moist deciduous and tropical semi-evergreen forests over the Central Highlands, Deccan Plateau and in northeast India. This was in line with the reports of FSI (2012, 2023) where border districts of Chhattisgarh, Madhya Pradesh, Andhra Pradesh, Odisha and northeast India have been reported to have the most fire incidences. A moderate fire pixel density (1.20–1.57 count·km $^{-2}$· yr^{-1}) was noted in tropical dry/moist deciduous and temperate evergreen forests including Eucalyptus and Pine plantations over Himalayan ranges in Uttarakhand and Nepal. On the contrary, forest over the western Himalaya including the Kashmir valley and in northern region of Pakistan and Afghanistan, and in Eastern part was found comparatively less fire prone. Moist deciduous forest over the north

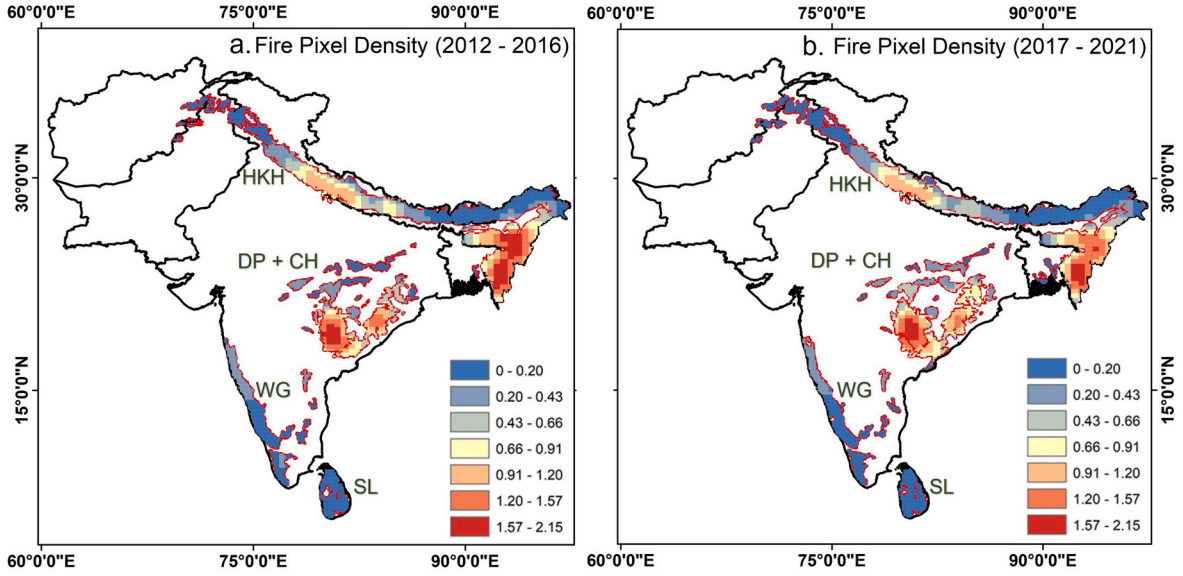

Fig. 4. The VIIRS fire pixel density averaged over individual forest system (unit: count · km $^{-2}$ · yr^{-1}).

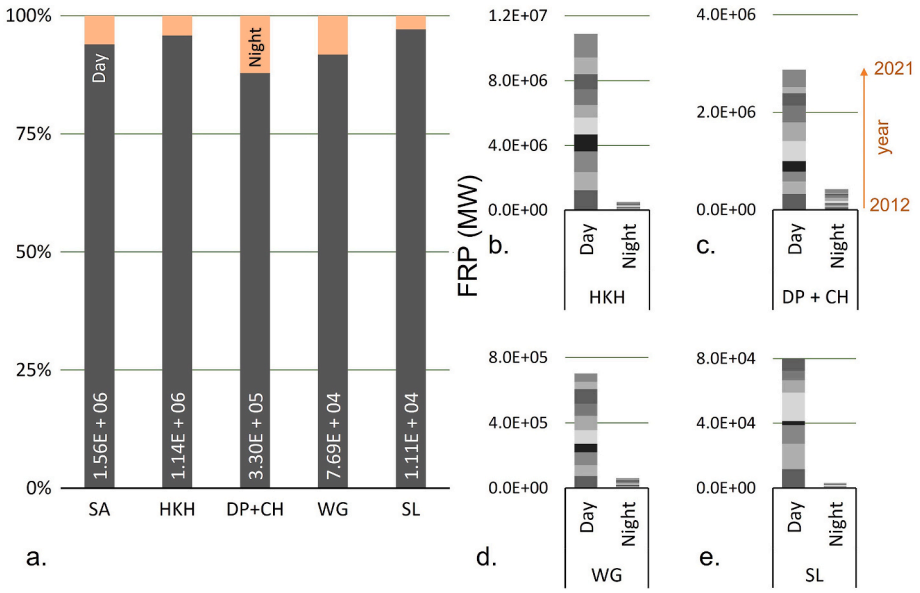

Fig. 5. Diurnal variations in fire radiative power, (a) day-night anomalies in percent contribution to annual mean FRP and (b–e) yearly accounts of day-night FRP. **NOTE**. Day-night aggregate FRP is marked in Fig. 5a with proportion (in %) retrieved between day and night overpass. Day-night resolved annual FRP from 2012 to 2021 over each forest system across South Asia is marked in Fig. 5b–d.

Western Ghats along the southwestern coast of Indian peninsula, especially over Indian state of Maharashtra and Karnataka, exhibited greater fire density compared to lower part. Such spatial heterogeneity is possibly related to more available moisture at root zone thereby, restricting fire to initiate and spread wildly.

The VIIRS I-band FRP i.e. spatial integration of energy (in MW) released per unit time from burning of biomass, and fire radiative energy (FRE) i.e. FRP integrated over time and space was assessed over forest land. In absence of time-resolved repeated observation on fire intensity to define energy emission from designated burnt area, we took day-night aggregate FRP as a proxy for total emission within a cross-section area. It should be noted that on a spatial scale FRP can be integrated to yield fire radiative energy when continuous data is available. Therefore, in many instances, geospatial modelling of fire emission was achieved reliably using FRP as a proxy of fire emission (Van Der Werf et al., 2017). As in Fig. S2, yearly variation in total FRP from each forest system did not yield significant variations. A MK test on annual FRP over South Asia yield insignificant trend with 0.02 MW decrease per year. Temporal variations in FRP among the forest cover is included in Fig. S3. Overall, 73% of aggregate FRP over South Asia (1.56×10^6 MW) was associated with the burning in HKH (1.14×10^6 MW) while rest of the forest system altogether accounted 25%, primarily linked to the forest over DP and CH (21%; 3.30×10^5 MW). On the contrary, a robust day and night variations in retrieved FRP was noted with disproportionate variation in FRP among the forest systems, as illustrated in Fig. 5. Approximately, >90% of aggregate FRP was linked with daytime retrieval, more intensively across HKH and in SL (>95%) compared to forest over CH and DP (87%; Table S4). Such discrepancy in retrieved FRP was likely associated to relatively much lower fire counts with small intensity fire during night compared to daytime. As in Fig. S4, nighttime fire counts and associated

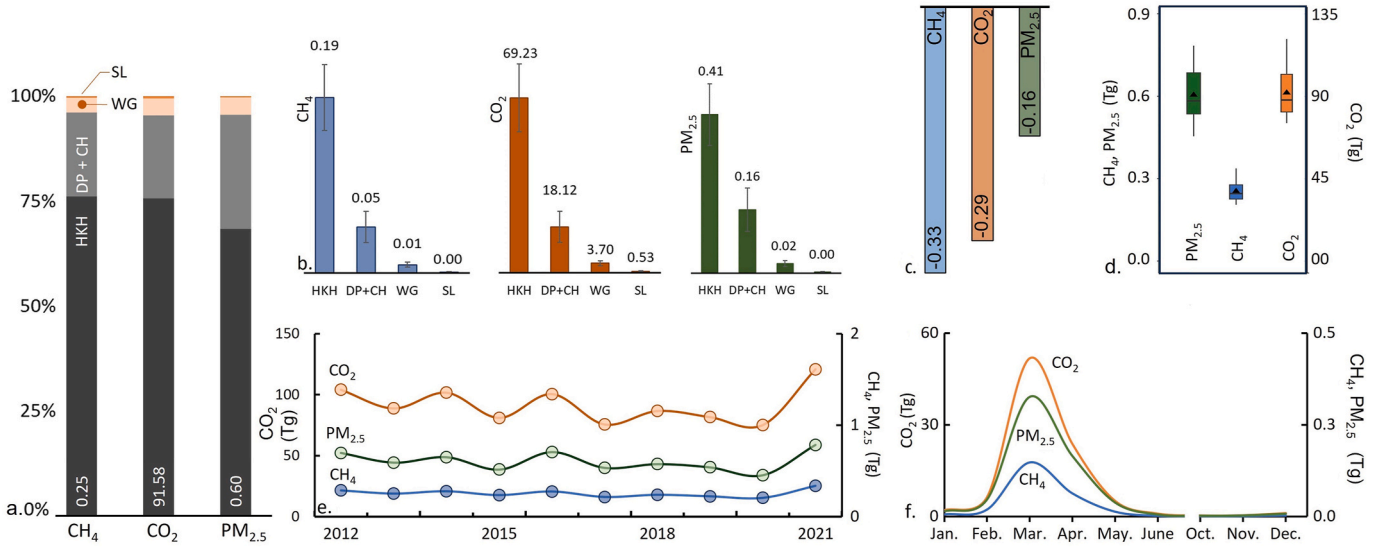

Fig. 6. Emission estimates of greenhouse gases and aerosols from forest fire across South Asia, (a) yearly emission estimate of CH_4, CO_2 and $PM_{2.5}$ with relative contributions of individual forest cover to total emission load (in %), (b) estimate of annual emission from individual forest cover, (c) decadal trend in emission for individual species, (d) variations in yearly emission estimates, (e) time-series of yearly emission rate in Tg yr^{-1} and (f) temporal variations in emission rate among the species in Tg $month^{-1}$.

NOTE. In Fig. 6a, the values placed at base in each bar denote total emissions in a year (in Tg yr^{-1}). The triangle and horizontal bar in Fig. 6d indicate mean and median, respectively. The lines were smoothed for better interpretation and visualization.

FRP appears much lower compared to daytime fire. Distinct diurnal variation in fire incidences is reported to associate with ecosystem type and primarily concentrate over the region where human induced forest fire predominates. Besides, Hély et al. (2003) concluded that during day time, relatively lower moisture content in biomass, wind profile and atmospheric temperature in general are more conducive to initiate greater fire occurrences compared to night. A similar robust diurnal variation in global forest fire both in MODIS and VIIRS thermal products was also accounted by Li et al. (2018).

3.4. Emission estimates of greenhouse gases and aerosols

3.4.1. Emission estimate of CO_2

Emission of greenhouse gases from fire in different forest system is documented globally, with specific focus on carbon-containing gases including CO_2, CH_4 and other organic/inorganic aerosols. Annual contribution of agriculture, forestry, and other land use changes accounts approximately 12 ± 4 Gt CO_2-eq emission that is roughly 20% of net global anthropogenic greenhouse gas emission (Pathak et al., 2022). Besides, fire contributes 5% of immediate direct CO_2 emission globally with annual C-emission varying from 1.8 to 2.0 Gt C yr^{-1} (Zheng et al., 2021). Understanding and quantifying the trends and drivers of forest fire in diverse forest covers across South Asia is therefore, imperative to recognize impacts of forest fire emissions on terrestrial C-budget. Fig. 6a indicates the annual emission rate of CO_2 from forest fire across South Asia with emission estimate constrained by individual forest cover and emission year. On the basis of VIIRS thermal anomaly and VFEI emission estimate, South Asia forest fire associated average CO_2 emission is likely to be 91.58 (±14.76) Tg yr^{-1}, with range varying from 75.14 to 120.80 Tg yr^{-1} in between 2012 and 2021, with a statistically insignificant (P: 0.05) decreasing trend of 0.03 yr^{-1}. Total C-emission, constraining both CO_2 and CH_4 emissions from forest fire would be in a range of 25.14 (±3.94) Tg C yr^{-1}, with a median value of 24.08 Tg C yr^{-1} accounting roughly 1.30% of global fire-related carbon emission in a year. This simply portrays the context that beside emission of several tons of C-containing greenhouse gases from conventional anthropogenic emission sources, emission from forest fire across South Asia do serves as a major emission sector for greenhouse gases, especially for the Carbon-containing trace gases. This becomes even more compelling considering the fact that approximately 70–80% of such forest fires are human induced and can be controlled by creating mass awareness and implying strict legalities.

A major fraction of CO_2 emission over South Asia was linked to forest fire over HKH mountain region, precisely because of its greater spatial extent, with annual CO_2 emission rate of 69.23 (±13.50) Tg, accounting 75.6% of total CO_2-emission associated to forest fire (Fig. 6b). Fire in broad leaf deciduous forests across DP + CH have annual CO_2-emission rate of 18.12 (±6.12) Tg, contributing roughly 19.8% of CO_2-emission of entire South Asia. Rest of the forest fire across Western Ghats and in Sri Lanka together accounts 4.6% of CO_2 emission, contributing 3.70 (±1.01) and 0.53 (±0.26) Gt CO_2 annually. In terms of relative contribution of C-containing greenhouse gases (like CH_4 and CO_2) on total carbon emission budget from South Asia forest fire (i.e., 25.14 Tg C yr^{-1}), emission from HKH accounts the major fraction (19.01 Tg yr^{-1}, 76%) followed by fire emissions from DP + CH (4.9 Tg yr^{-1}, 20%) while emissions from WG and SL share the remaining 4% of C-emission. Our results reciprocate well with the previous observation on high carbon emission from eastern Himalayan states by Sannigrahi et al. (2020) and considerably higher than CO_2 emission rate (3.83 Tg yr^{-1}) reported from forest fire in mainland China (Fan et al., 2024). Interannual variation in fire associated CO_2 emission (Fig. 6e) does not indicate any robust trend. Intraannual variation in emission however, strictly suggest that the major proportion of CO_2 emission is linked to peak fire incidence period (Fig. S5), with highest being in March as the case in VIIRS forest fire counts, with consequent decrease in emissions as the monsoonal rain dominates over the South Asia. A robust variation in temporal emission pattern of CO_2 is a signature of south Asian forest fire which peak during February to May. We note, February to May fire season accounts 90% of fire counts and 95% of CO_2 annual emissions over South Asia.

3.4.2. Emission estimate of CH_4

Contribution of forest fire to regional emission of CH_4, a more potent greenhouse gas compared to CO_2, was also assessed. Estimates of cumulative annual emissions of CH_4 is included in Fig. 6. In a given year, a total of 0.25 (±0.04) Tg of CH_4 was estimated to be emitted from forest fire across South Asia with equivalent carbon emission of 0.19 Tg yr^{-1}.

Overall, forest fire specific CH_4 emission denote a statistically insignificant (*P: 0.05*) decreasing trend with 0.03 decline in emission each year. Like CO_2, robust variations in CH_4 emission across forests system was also accounted with major proportion (77%) of CH_4 originating from the fire across HKH, followed by fire across DP + CH (20%). Approximately, 96% of annual CH_4 emission was linked to emission during peak fire season (February–May), with 60% of emission solely in the month of March. There are global reports of CH_4 emission from the forest fire with marked spatial biases and uncertainties. Liu et al. (2020) compared several inventories on CH_4 emission from global fire database and reported 33% coefficient of variation among the estimates between inventories. A range in between 15 and 30 Tg yr^{-1} CH_4 emission was reported using MODIS based burnt area and fire counts. Fan et al. (2021) accounted 0.02 Tg yr^{-1} emission of CH_4 from forest fire across China using MODIS based burnt area and land cover map. With similar MODIS based fire product, Shi et al. (2015) noted 30 Tg yr^{-1} CH_4 emissions solely from the biomass burning over the tropical region. Emission estimate of CH_4 based on VFEI inventory corresponds well with emission from other regional sectors, but requires further refinement of the data product to consider diurnal fluctuation.

3.4.3. Emission estimate of $PM_{2.5}$

Incomplete combustion of lignocellulosic biomass including cellulose, hemicellulose, and lignin are also responsible for emission of fine particulates. Forest fire across South Asia was found to emit 0.60 (±0.10) Tg yr^{-1} $PM_{2.5}$ varying considerably across the forest biomes (Fig. 7). Fire specific yearly emission of $PM_{2.5}$ denote a statistically insignificant decreasing trend (−0.02 yr^{-1}) in emission per year. A strong heterogeneity in forest fire emissions across forest cover was also noted. Fire over the HKH accounted 68% of aggregate $PM_{2.5}$ emission from South Asia, with annual rate of 0.41 (±0.08) Tg $PM_{2.5}$. Besides HKH, forest fire over DP + CH accounts 27% of aggregate $PM_{2.5}$ emissions with annual rate of 0.16 (±0.06) Tg. Like the emission of other co-emitting trace gases, fire season during February to May accounts 95% of $PM_{2.5}$ emission (0.57 Tg), particularly in the month of March. When compared with open biomass burning emissions of $PM_{2.5}$ from the entire South and Southeast Asia except northern parts of HKH (70°–130° E, 0°-28° N), Ferrada et al. (2022) reported an annual $PM_{2.5}$ emission of approx. 4 Tg, with emissions predominately linked to peat fires over Indonesia and Malaysia.

3.5. Uncertainly in forest fire emission estimate

Several uncertainties remain in estimating emission from biomass-based fire, be it a top-down (FRP based) or bottom-up approach (burnt area). It is noteworthy that biomass-based emission inventories rely on certain products, either by space-borne sensors or by ground-based measurements, and none of them provide immediate observation of the emission profile of a species. Technically, each of the biomass based inventories confer generalization of emission estimates from lab experiments or from in-situ observation. Such emission flux may markedly vary with time and space, and it is extremely challenging to evaluate its appropriateness over individual biome. Another potential source of error is the cloud contamination of fire pixels when sensed using space borne sensor. Likewise, VFEI does not incorporate refinement of fires potentially obscured by clouds, leading to reduced emission estimate over selected biomes, especially over the Siberia and Boreal America (Ferrada et al., 2022). Another limitation could be the unavailability of sub-daily emission estimates at global level as forest fires do pose diurnal cycle which potentially impact the resultant emission. In VFEI, a Gaussian distribution with fire peak at 14:00 local time is included (Ferrada et al., 2022), which could inherit considerable diurnal bias for the large fires. An infrequent VIIRS overpass compared to MODIS also generalizes FRP estimates in VIIRS fire products which was however, overcome by including a scaling factor irrespective of forest biomes. Inclusion of a universal scaling factor does require additional research for local optimization. Besides, a biome specific adjustment factors was not also included in VFEI deliberating its application for global modelling studies.

4. Conclusions

Biomass burning emissions have been reported to contribute significant amount of carbon-containing greenhouse gases, aerosols, and its precursor species in to the Earth's atmosphere which in turn reduce the extent of ecosystem services of forest by sequestering carbon within the biomass itself. Here, attempt has been made to quantify the emissions of greenhouse gases like CO_2 and CH_4, and aerosols (as $PM_{2.5}$) from the year-long burning of forest fire across South Asia. Initially, Suomi-NPP onboard VIIRS sensor I-band active fire products and thermal anomalies were retrieved for the years 2012–2021 (except monsoon months) to assess geospatial variations of fire incidences and fire radiative power across South Asia. Further, VIIRS-based biomass burning high-resolution emission inventory was followed to quantify possible emissions of trace gases and aerosols. Our attempt is novel considering no prior reports on forest fire emissions across South Asia which could well be utilized for developing mitigation strategies and improved parameterization of regional climate and air quality models.

Initially, forest cover across South Asia was mapped using Terra/Aqua MODIS land cover data product. Forest cover was spatially subdivided into four forest systems to ascertain geospatial variations in fire incidences and associated emissions. On an average, forest across

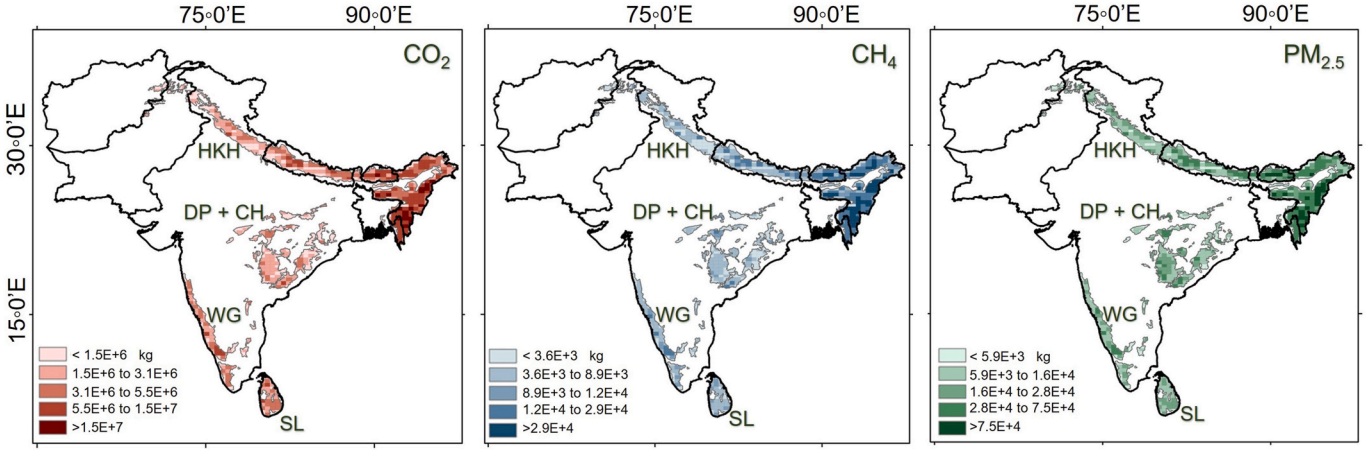

Fig. 7. Geospatial variations in forest fire emission estimates (in kg yr^{-1}) of greenhouse gases and aerosols across South Asia.

South Asia experiences 0.17 (±0.05) million (M) fire incidences, majority of which occurred in forest across Hindu Kush Himalaya (HKH, 56%), followed by Central Highlands (CH) and Deccan Plateau (DP, 36%). Most of these fire incidences were however, linked to high temperature, fuel availability and biomass dryness coupled with human influences. A marked seasonality in fire incidences were also noted with fire predominately retrieved in between February and May with higher radiative power compared to wider prevalence of very small and less intense fires during October to January months. The tropical dry/moist deciduous and semi-evergreen forests over the Central Highlands, Deccan Plateau and in northeast India were most prone to frequent fire incidences. A robust diurnal variation in fire radiative power was also accounted in VIIRS retrievals which was explained by the incidence of relatively lower fire counts and small intensity fire during night compared to daytime.

Forest fire across South Asia contribute approximately 1.3% of global carbon containing greenhouse gas emissions with annual emission in a range of 25.14 (±3.94) Tg C year^{-1}, and a median of 24.14 Tg C year^{-1}. Majority of such carbon was associated to emission of CO_2 with prime contribution from fire across HKH forest and forest fire over Central Highlands and Deccan Plateau. Emission of CH_4 from fire also reciprocate the similar trend with annual emission rate of 0.25 (±0.04) Tg and equivalent carbon emission of 0.19 Tg yr^{-1}. In terms of $PM_{2.5}$, fire associated emission rate was 0.60 (±0.10) Tg yr^{-1} with major contribution from forest fire across HKH and Central Highlands and Deccan Plateau. Yearly emission rate of all the species however, accounts statistically insignificant declining trend. On closing, despite having many uncertainties in estimating biomass burning emissions either by using space-borne sensor or in-situ experiments, these biomass burning inventories serves well in estimating emissions from fires across varying landscape. Our analysis provides a brief overview on how such emissions varies across geographical region in South Asia and could well be useful for fire management and in reducing emissions.

CRediT authorship contribution statement

Kumari Aditi: Visualization, Validation, Methodology, Formal analysis, Data curation. **Akanksha Pandey:** Investigation, Formal analysis, Data curation. **Tirthankar Banerjee:** Writing – original draft, Visualization, Supervision, Software, Resources, Methodology, Investigation, Funding acquisition, Conceptualization.

Declaration of competing interest

The authors declare that they have no known competing financial interests or personal relationships that could have appeared to influence the work reported in this paper.

Acknowledgments

The research is partially supported by the Banaras Hindu University under Institute of Eminence grant (6031). Authors would like to thank the VIIRS Science Team for processing and maintaining VIIRS thermal anomaly and fire data, and VFEI team for creation and dissemination of biomass-based fire emission inventory data. Authors also acknowledge the suggestions provided by two anonymous reviewers.

Appendix A. Supplementary data

Supplementary data related to this article can be found at https://doi.org/10.1016/j.envpol.2024.125441.

Data availability statement

The VIIRS Collection 2 VNP14IMG - VIIRS/NPP Active Fires 6-Min L2 Swath 375m data is available from https://ladsweb.modaps.eosdis.nasa.gov/archive, last accessed on August 15, 2024. The VIIRS-based fire emission inventory data is available from a dedicated server of the University of Iowa (http://bio.cgrer.uiowa.edu/VFEI/DOWNLOAD, last access: March 10, 2024). TERRA/AQUA MODIS Land Cover Type Yearly Level-3 Global product of 500 m spatial resolution is available at https://ladsweb.modaps.eosdis.nasa.gov/. Forest area database was collected from https://data.worldbank.org/last accessed on March 20, 2024.

References

Abatzoglou, J.T., Kolden, C.A., 2013. Relationships between climate and macroscale area burned in the western United States. Int. J. Wildland Fire 22, 1003–1020.
Andela, N., van der Werf, G.R., 2014. Recent trends in African fires driven by cropland expansion and El Niño to La Niña transition. Nat. Clim. Change 4, 791–795.
Andreae, M.O., 2019. Emission of trace gases and aerosols from biomass burning – an updated assessment. Atmos. Chem. Phys. 19, 8523–8546.
Badarinath, K.V.S., Sharma, A.R., Kharol, S.K., 2011. Forest fire monitoring and burnt area mapping using satellite data: a study over the forest region of Kerala State, India. Int. J. Rem. Sens. 32 (1), 85–102.
Bajracharya, K.M., 2002. Forest fire situation in Nepal. International Forest Fire News 26, 84–86.
Bian, H., Chin, M., Kawa, S., Duncan, B., Arellano, A., Kasibhatla, P., 2007. Sensitivity of global CO simulations to uncertainties in biomass burning sources. J. Geophys. Res. Atmos. 112, 866.
Bowman, D.M., Kolden, C.A., Abatzoglou, J.T., Johnston, F.H., van der Werf, G.R., Flannigan, M., 2020. Vegetation fires in the anthropocene. Nat. Rev. Earth Environ. 1 (10), 500–515.
Chen, Y., Romps, D.M., Seeley, J.T., Veraverbeke, S., Riley, W.J., Mekonnen, Z.A., Randerson, J.T., 2021. Future increases in Arctic lightning and fire risk for permafrost carbon. Nat. Clim. Change 11 (5), 404–410.
Clarke, H., Nolan, R.H., De Dios, V.R., Bradstock, R., Griebel, A., Khanal, S., Boer, M.M., 2022. Forest fire threatens global carbon sinks and population centres under rising atmospheric water demand. Nat. Commun. 13 (1), 7161.
Csiszar, I., Schroeder, W., Giglio, L., Ellicott, E., Vadrevu, K.P., Justice, C.O., Wind, B., 2014. Active fires from the Suomi NPP visible infrared imaging radiometer suite: product status and first evaluation results. J. Geophys. Res. Atmos. 119, 803–816.
Deb, P., Moradkhani, H., Abbaszadeh, P., Kiem, A.S., Engström, J., Keellings, D., Sharma, A., 2020. Causes of the widespread 2019–2020 Australian bushfire season. Earth's Future 8 (11).
Duff, T.J., Penman, T.D., 2021. Determining the likelihood of asset destruction during wildfires: modelling house destruction with fire simulator outputs and local-scale landscape properties. Saf. Sci. 139, 105196.
Fan, B., Ciais, P., Chevallier, F., Chuvieco, E., Chen, Y., Yang, H., 2021. Increasing forest fire emissions despite the decline in global burned area. Sci. Adv. 7 (39), eabh2646.
Fan, D., Wang, M., Liang, T., He, H., Zeng, Y., Fu, B., 2024. Estimation and trend analysis of carbon emissions from forest fires in mainland China from 2011 to 2021. Ecol. Inf. 81, 102572.
FAO, 2020a. Global forest Resources assessment 2020 – key findings. Rome. https://doi.org/10.4060/ca8753en.
FAO, 2020b. Global forest Resources assessment 2020: main report. Rome. Available at: https://doi.org/10.4060/ca9825en . (Accessed 12 April 2024).
Ferrada, G.A., Zhou, M., Wang, J., Lyapustin, A., Wang, Y., Freitas, S.R., Carmichael, G. R., 2022. Introducing the VIIRS-based fire emission inventory version 0 (VFEIv0). Geosci. Model Dev. (GMD) 15 (21), 8085–8109.
Field, R.D., Van der Werf, G.R., Shen, S.S., 2009. Human amplification of drought-induced biomass burning in Indonesia since 1960. Nat. Geosci. 2 (3), 185–188.
FSI, 2012. Vulnerability of India's Forests to Fires. Forest Survey of India (FSI). Available at. Ministry of Environment, Forest, and Climate Change of the Government of India, New Delhi https://fsi.nic.in/index.php/. (Accessed 1 March 2024).
FSI, 2019. India State of Forest Report 2019, Forest Survey of India, Ministry of Environment, Forest and Climate Change (MoEFCC). Government of India.
FSI, 2020. Rapid assessment of fire affected forest areas in the country based on MODIS-detections following a sampling approach. ISBN: 978-81-941018-5-7. Available at. In: FSI Technical Information Series, Forest Survey of India (FSI). Ministry of Environment, Forest, and Climate Change of the Government of India, New Delhi https://fsi.nic.in/fsi-result/technical-information-series-vol2-no2-2020.pdf. (Accessed 10 April 2024).
FSI, 2023. The India State of Forest Report. Forest Survey of India (FSI). Ministry of Environment, Forest, and Climate Change of the Government of India, New Delhi. https://fsi.nic.in/isfr-2021/. (Accessed 10 April 2024).
Gale, M.G., Cary, G.J., Van Dijk, A.I., Yebra, M., 2021. Forest fire fuel through the lens of remote sensing: review of approaches, challenges and future directions in the remote sensing of biotic determinants of fire behaviour. Rem. Sens. Environ. 255, 112282.
Giglio, L., Boschetti, L., Roy, D.P., Humber, M.L., Justice, C.O., 2018. The collection 6 MODIS burned area mapping algorithm and product. Remote Sens. Environ. 217, 72–85.
Giglio, L., Csiszar, I., Justice, C.O., 2006. Global distribution and seasonality of active fires as observed with the Terra and aqua moderate resolution imaging spectroradiometer (MODIS) sensors. J. Geophys. Res. 111, G02016.
Goldberg, M.D., Kilcoyne, H., Cikanek, H., Mehta, A., 2013. Joint Polar Satellite System: the United States next generation civilian polar orbiting environmental satellite system. J. Geophys. Res. 118 (13,463–13), 475.

Hely, C., Alleaume, S., Swap, R.J., Shugart, H.H., Justice, C.O., 2003. SAFARI 2000 characterization of fuels, fire behavior, combustion completeness, and emissions from experimental burns in infertile grass savannas in western Zambia. J. Arid Environ. 54, 381–394, 2003.

Hua, W., Lou, S., Huang, X., Xue, L., Ding, K., Wang, Z., Ding, A., 2023. Diagnosing Uncertainties in Global Biomass Burning Emission Inventories and Their Impact on Modeled Air Pollutants. EGUsphere. https://doi.org/10.5194/egusphere-2023-1822 [preprint].

Ichoku, C., Kaufman, Y.J., 2005. A method to derive smoke emission rates from MODIS fire radiative energy measurements. IEEE Trans. Geosci. Rem. Sens. 43 (11), 2636–2649.

Jerrett, M., Jina, A.S., Marlier, M.E., 2022. Up in smoke: California's greenhouse gas reductions could be wiped out by 2020 wildfires. Environ. Pollut. 310, 119888.

Kaufman, Y.J., Justice, C.O., Flynn, L.P., Kendall, J.D., Prins, E.M., Giglio, L., et al., 1998. Potential global fire monitoring from EOS-MODIS. J. Geophys. Res. 103 (32), 238, 215–32.

Kumar, S.S., Roy, D.P., Boschetti, L., Kremens, R., 2011. Exploiting the power law distribution properties of satellite fire radiative power retrievals: a method to estimate fire radiative energy and biomass burned from sparse satellite observations. J. Geophys. Res. 116, D19303.

Li, F., Zhang, X., Kondragunta, S., Csiszar, I., 2018. Comparison of fire radiative power estimates from VIIRS and MODIS observations. J. Geophys. Res. Atmos. 123 (9), 4545–4563.

Liu, T., Mickley, L.J., Marlier, M.E., DeFries, R.S., Khan, M.F., Latif, M.T., Karambelas, A., 2020. Diagnosing spatial biases and uncertainties in global fire emissions inventories: Indonesia as regional case study. Rem. Sens. Environ. 237, 111557.

McLauchlan, K.K., Higuera, P.E., Miesel, J., Rogers, B.M., Schweitzer, J., Shuman, J.K., Tepley, A.J., Varner, J.M., Veblen, T.T., Adalsteinsson, S.A., Balch, J.K., 2020. Fire as a fundamental ecological process: research advances and frontiers. J. Ecol. 108, 2047–2069.

Mina, U., Dimri, A.P., Farswan, S., 2023. Forest fires and climate attributes interact in central Himalayas: an overview and assessment. Fire Ecology 19 (1), 14.

Moritz, M.A., Morais, M.E., Summerell, L.A., Carlson, J.M., Doyle, J., 2005. Wildfires, complexity, and highly optimized tolerance. Proceedings of the National Academy of Sciences of the United States of America 102 (50), 17,912–17,917.

Negi, G.C.S., Dhyani, P.P., 2012. Glimpses of Forestry Research in the Indian Himalayan Region. Almora: Pant Institute of Himalayan Environment and Development.

Nguyen, H.M., Wooster, M.J., 2020. Advances in the estimation of high Spatio-temporal resolution pan-African top-down biomass burning emissions made using geostationary fire radiative power (FRP) and MAIAC aerosol optical depth (AOD) data. Remote Sens. Environ. 248, 111971.

Oliva, P., Schroeder, W., 2015. Atmospheric correction of VIIRS and MODIS fire radiative power retrievals for multi-sensor comparison, paper presented at 2015. IEEE International Geoscience and Remote Sensing Symposium (IGARSS), 26-31 July 2015.

Pan, X., Ichoku, C., Chin, M., Bian, H., Darmenov, A., Colarco, P., Ellison, L., Kucsera, T., da Silva, A., Wang, J., Oda, T., 2020. Six global biomass burning emission datasets: intercomparison and application in one global aerosol model. Atmos. Chem. Phys. 20 (2), 969–994.

Pathak, M., Slade, R., Pichs-Madruga, R., Ürge-Vorsatz, D., Shukla, R., Skea, J., 2022. Climate Change 2022 Mitigation of Climate Change. Technical Summary.

Polivka, T., Wang, J., Ellison, L., Hyer, E., Ichoku, C., 2016. Improving nocturnal fire detection with the VIIRS day-night band. IEEE Trans. Geosci. Remote Sens. 9, 5503–5519.

Prasad, V.K., Badarinath, K.V.S., Eaturu, A., 2008. Biophysical and anthropogenic controls of forest fires in the Deccan Plateau, India. J. Environ. Manag. 86 (1), 1–13.

Ramakrishnan, P.S., Rao, K.S., Chandrashekara, U.M., Chhetri, N., Gupta, H.K., Patnaik, S., Saxena, K.G., Sharma, E., 2012. South Asia. In: Parrotta, J.A., Trosper, R. L. (Eds.), Traditional Forest-Related Knowledge: Sustaining Communities, Ecosystems and Biocultural Diversity, World Forests, vol. 12. https://doi.org/10.1007/978-94-007-2144-9_9.

RGoB, 2004. Annual Forest Fire Evaluation and Compilation Report. MOA, SFD/FFMS Royal Government of Bhutan, Thimphu, Bhutan.

Roteta, E., Bastarrika, A., Padilla, M., Storm, T., Chuvieco, E., 2019. Development of a Sentinel-2 burned area algorithm: generation of a small fire database for sub-Saharan Africa. Remote Sens. Environ. 222, 1–17.

Roy, D.P., Huang, H., Boschetti, L., Giglio, L., Yan, L., Zhang, H.K., Li, Z., 2019. Landsat-8 and Sentinel-2 burned area mapping - a combined sensor multi-temporal change detection approach. Remote Sens. Environ. 231, 111254.

Sannigrahi, S., Pilla, F., Basu, B., Basu, A.S., Sarkar, K., Chakraborti, S., Joshi, P.K., Zhang, Q., Wang, Y., Bhatt, S., Bhatt, A., 2020. Examining the effects of forest fire on terrestrial carbon emission and ecosystem production in India using remote sensing approaches. Sci. Total Environ. 725, 138331.

Schroeder, W., Oliva, P., Giglio, L., Csiszar, I.A., 2014. The New VIIRS 375m active fire detection data product: algorithm description and initial assessment. Remote Sens. Environ. 143, 85–96.

Shi, Y., Matsunaga, T., Yamaguchi, Y., 2015. High-resolution mapping of biomass burning emissions in three tropical regions. Environmental science & technology 49 (18), 10806–10814.

Smith, A.M.S., Wooster, M.J., 2005. Remote classification of head and backfire types from MODIS fire radiative power and smoke plume observations. Int. J. Wildland Fire 14, 249–254.

Touma, D., Stevenson, S., Lehner, F., Coats, S., 2021. Human-driven greenhouse gas and aerosol emissions cause distinct regional impacts on extreme fire weather. Nat. Commun. 12 (1), 212.

Vadrevu, K.P., Ellicott, E., Giglio, L., Badarinath, K.V.S., Vermote, E., Justice, C., Lau, W. K., 2012. Vegetation fires in the himalayan region–Aerosol load, black carbon emissions and smoke plume heights. Atmos. Environ. 47, 241–251.

Vadrevu, K., Lasko, K., 2018. Intercomparison of MODIS AQUA and VIIRS I-Band fires and emissions in an agricultural landscape—implications for air pollution research. Rem. Sens. 10 (7), 978.

Vadrevu, K.P., Lasko, K., Giglio, L., Schroeder, W., Biswas, S., Justice, C., 2019. Trends in vegetation fires in south and southeast Asian countries. Sci. Rep. 9 (1), 7422.

van der Velde, I.R., van der Werf, G.R., Houweling, S., Maasakkers, J.D., Borsdorff, T., Landgraf, J., Tol, P., van Kempen, T.A., van Hees, R., Hoogeveen, R., Veefkind, J.P., 2021. Vast CO2 release from Australian fires in 2019–2020 constrained by satellite. Nature 597 (7876), 366–369.

van der Werf, G.R., Randerson, J.T., Giglio, L., Collatz, G.J., Mu, M., Kasibhatla, P.S., Morton, D.C., DeFries, R.S., Jin, Y.V., van Leeuwen, T.T., 2010. Global fire emissions and the contribution of deforestation, savanna, forest, agricultural, and peat fires (1997–2009). Atmos. Chem. Phys. 10 (23), 11707–11735.

van der Werf, G.R., Randerson, J.T., Giglio, L., Van Leeuwen, T.T., Chen, Y., Rogers, B. M., Mu, M., Van Marle, M.J., Morton, D.C., Collatz, G.J., Yokelson, R.J., 2017. Global fire emissions estimates during 1997–2016. Earth Syst. Sci. Data 9 (2), 697–720.

Vermote, E., Ellicott, E., Dubovik, O., Lapyonok, T., Chin, M., Giglio, L., Roberts, G.J., 2009. An approach to estimate global biomass burning emissions of organic and black carbon from MODIS fire radiative power. J. Geophys. Res. Atmos. 114 (D18).

Wang, J., Yue, Y., Wang, Y., Ichoku, C., Ellison, L., Zeng, J., 2018. Mitigating satellite-based fire sampling limitations in deriving biomass burning emission rates: application to WRF-chem model over the northern sub-saharan African region. J. Geophys. Res. Atmos. 123, 507–528.

Wooster, M.J., Roberts, G.J., Giglio, L., Roy, D.P., Freeborn, P.H., Boschetti, L., Justice, C., Ichoku, C., Schroeder, W., Davies, D., Smith, A.M., 2021. Satellite remote sensing of active fires: history and current status, applications and future requirements. Rem. Sens. Environ. 267, 112694.

Wooster, M.J., Zhukov, B., Oertel, D., 2003. Fire radiative energy for quantitative study of biomass burning: derivation from the BIRD experimental satellite and comparison to MODIS fire products. Remote Sens. Environ. 86, 83–107.

World Bank, 2024. World development indicators. South Asia - forest area. Available at: https://data.worldbank.org/indicator/AG.LND.FRST.ZS?end=2021&locations=8S&start=2021FAO . (Accessed 20 January 2024).

Xu, R., Yu, P., Abramson, M.J., Johnston, F.H., Samet, J.M., Bell, M.L., Haines, A., Ebi, K. L., Li, S., Guo, Y., 2020. Wildfires, global climate change, and human health. N. Engl. J. Med. 383 (22), 2173–2181.

Zheng, B., Ciais, P., Chevallier, F., Chuvieco, E., Chen, Y., Yang, H., 2021. Increasing forest fire emissions despite the decline in global burned area. Sci. Adv. 7 (39), eabh2646.